Small angle neutron scattering investigation of partially crystallized $Fe_{76.5-x}Si_{15.5}B_7CuNb_x$ alloys

1998 J. Phys.: Condens. Matter 10 5267

(http://iopscience.iop.org/0953-8984/10/24/005)

J. Phys.: Condens. Matter **10** (1998) 5267–5276. Printed in the UK PII: S0953-8984(98)89898-6

Small angle neutron scattering investigation of partially crystallized $Fe_{76.5-x}Si_{15.5}B_7CuNb_x$ alloys

A Danzig†§, A Wiedenmann† and N Mattern‡

† HMI Berlin, Glienickerstrasse 100, 14109 Berlin, Germany
‡ IFW Dresden, PF, 01171 Dresden, Germany

Received 9 December 1997, in final form 26 February 1998

Abstract. Fluctuations in the nuclear scattering density and magnetization in partially crystallized alloys with composition $Fe_{76.5-x}Si_{15.5}B_7CuNb_x$ were investigated by means of small angle neutron scattering. From nuclear and magnetic scattering the size distributions of nanocrystals were determined as a function of the annealing temperature and the concentration of niobium.

1. Introduction

FeSiB based alloys with additions of copper and niobium show after thermal treatment at 550 °C good soft magnetic properties [1] due to the formation of nanocrystalline ferromagnetic α-(Fe,Si) precipitates. The correlation between particle size, magnetostriction, permeability and coercive force [2] was described on the basis of the random anisotropy model [3]. Niobium impedes particle growth [4], but only for simultaneous addition of copper does a broad temperature range of coexistence between amorphous phase and nanocrystals [5] exist. In numerous papers the influence of the chemical composition on microstructure and magnetic properties was investigated [6–9]. From the knowledge of the size distribution of crystals it should be possible to understand the mechanism of nucleation and crystal growth. Unfortunately, the determination of size distributions is connected with considerable problems. From x-ray diffraction (XRD) only a mean particle size can be estimated, whereas for transmission electron microscopy (TEM) the small irradiated sample volume prevents a reliable determination of the size distributions. Small angle neutron scattering (SANS) was used to determine the size distributions of nanocrystals after annealing of $Fe_{76.5-x}Si_{15.5}B_7CuNb_x$ alloys with systematic variation of the Nb content. SANS includes large sample volumes (2 mm^3) and allows simultaneous studies of magnetic fluctuations.

2. Experiment

The amorphous alloys with a thickness of 20 μm, produced at the IFW Dresden by means of melt-spinning, were thermally annealed under H_2 atmosphere. X-ray diffraction was measured at a vertical diffractometer PW1820 (Philips). SANS was performed at the

§ Corresponding author: Hahn-Meitner-Institut Berlin, Dept. NE, Glienickerstrasse 100, 14109 Berlin, Germany. Tel: +49 (0)30 8062 3177. Fax: +49 (0)30 8062 2999. E-mail address: danzig@hmi.de

0953-8984/98/245267+10$19.50

instrument V4 installed at the research reactor BERII in Berlin [10]. Cold neutrons with a wavelength $\lambda = 0.6$ nm and $\Delta\lambda/\lambda = 0.1$ were selected from the rotating velocity selector. The samples were cut into 10 mm × 10 mm pieces. They were placed inside a vacuum chamber containing an electromagnet with horizontal magnetic field up to 1 T applied perpendicular to the incident neutron beam and parallel to the surface of the samples. We used a two-dimensional detector with 4096 cells of 1 cm^2 each perpendicular to the incident beam. Three sample–detector distances (2, 4 and 12 m) were selected to extend the observable range of momentum transfer.

3. Results and discussion

3.1. XRD

X-ray diffraction confirmed that all samples were amorphous in the as-quenched state. From the intensities and the broadening of the Bragg peaks we calculated the crystalline volume fractions and mean particle sizes L (table 1) of the partially crystallized samples. The quantity L is the volume average of the crystal dimension in the direction perpendicular to the diffracting planes [11]. For an ensemble of spheres with diameter D the mean size is expressed by $L = \frac{3}{4}\langle D^4\rangle/\langle D^3\rangle$.

Table 1. Crystalline volume fraction x_c and mean particle size L determined from XRD in dependence on chemical composition and annealing conditions.

	Annealing conditions			
Alloy	T_A (°C)	t_A (h)	x_c	L (nm)
$Fe_{75.5}Si_{15.5}B_7CuNb_1$	500	1	0.78	29
$Fe_{74.5}Si_{15.5}B_7CuNb_2$	550	1	0.78	19
$Fe_{73.5}Si_{15.5}B_7CuNb_3$	475	6	0.38	14
$Fe_{73.5}Si_{15.5}B_7CuNb_3$	500	1	0.45	14
$Fe_{73.5}Si_{15.5}B_7CuNb_3$	550	1	0.67	14
$Fe_{71.5}Si_{15.5}B_7CuNb_5$	550	1	0.45	14

In $Fe_{73.5}Si_{15.5}B_7CuNb_3$ a mean particle size of 14 nm was found independent of the temperature. The transformed volume fraction increases with the annealing temperature due to an increased number density of particles. For higher Nb concentration the particle size remains unchanged, but compared with $x = 3$ at.% the crystalline volume is lower and indicates a reduced nucleation rate. A comparison between $x = 2$ and 3 at.% annealed at 550 °C as well as $x = 1$ and 3 at.% annealed at 500 °C shows the following behaviour. If the niobium content is reduced, then the particle size increases. Furthermore the transformed volume increases. Nb influences both nucleation and crystal growth.

3.2. SANS results

3.2.1. Nuclear and magnetic contribution. Local fluctuations in the nuclear scattering length density caused by variations in the density or chemical composition give rise to a SANS signal. Besides this nuclear contribution the magnetic moment of the neutron leads to magnetic scattering for samples with magnetic inhomogeneities. Magnetic scattering measures fluctuations of both the orientation and the magnitude of the magnetization density

$\boldsymbol{M}(\boldsymbol{r})$. The total SANS signal depends on the magnitude Q of the scattering vector $\boldsymbol{Q}$ and the angle Ψ between the scattering vector and the external magnetic field $\boldsymbol{B}_0$:

$$I(Q, \Psi) = A(Q) + B(Q) \sin^2 \Psi. \tag{1}$$

For randomly distributed and oriented particles embedded in a homogeneous matrix nuclear scattering becomes purely isotropic. However, the behaviour of magnetic scattering depends on the orientation of the magnetic moments. For random orientation of all magnetic moments the magnetic scattering signal also becomes isotropic. $B(Q)$ vanishes and $A(Q)$ includes nuclear and magnetic scattering. For magnetic saturation when all moments are aligned, the magnetic scattering contribution is described by $|M(Q)|^2 \sin^2 \Psi$ [12]. $A(Q)$ corresponds to nuclear and $B(Q)$, which is proportional to the Fourier transform of $\boldsymbol{M}(\boldsymbol{r})$, to magnetic scattering. In between these extrema the magnetic scattering is included in $A(Q)$ and $B(Q)$.

We measured for all samples the two dimensional scattering patterns. Figure 1 shows the contourplot for $Fe_{71.5}Si_{15.5}B_7CuNb_5$ (550 °C/1 h) without external magnetic field and in magnetic saturation. From radial fitting of the angular dependence (1) for magnetic saturation we determined the nuclear and magnetic contributions $A(Q)$ and $B(Q)$, which are plotted as a function of the momentum transfer Q in figure 2. In $Fe_{75.5}Si_{15.5}B_7CuNb_1$ $A(Q)$ and $B(Q)$ increase with decreasing Q. Even in the as-quenched state we found significant scattering intensities below 0.2 nm^{-1} due to long range fluctuations. We assume that they are induced during melt spinning and affect nuclear scattering at low Q much more than the magnetic contribution. For all other samples a pronounced maximum occurs near $Q = 0.4$ nm^{-1} in the magnetic contribution. The nuclear contribution $A(Q)$ shows only some kind of plateau near $Q = 0.4$ nm^{-1}; out of this region the intensity increases continuously with decreasing Q. The height of the peak in $B(Q)$ depends on the sample composition, which influences the scattering contrast, and the crystallization degree. The presence of the maximum in the scattering curves may arise from: (i) interference of the scattering waves emitted from different particles and/or (ii) a concentration profile around the particles. In the next section both effects are considered in detail by means of simple simulations. For the samples $Fe_{73.5}Si_{15.5}B_7CuNb_3$ the peak becomes more pronounced if the temperature increases from 500 to 550 °C, whereas in the ranges $Q < 0.2$ nm^{-1} and

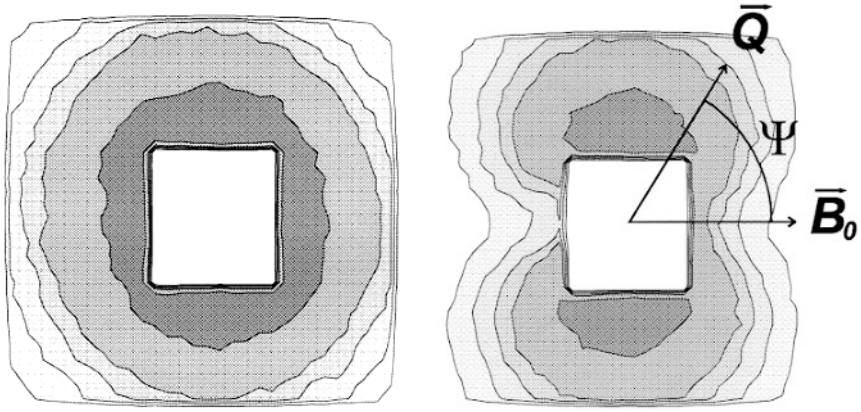

Figure 1. Intensity contourplot of the SANS pattern of $Fe_{71.5}Si_{15.5}B_7CuNb_5$ (550 °C/1 h) with (*a*) $B_0 \cong 0$ and (*b*) $B_0 = 1$ T.

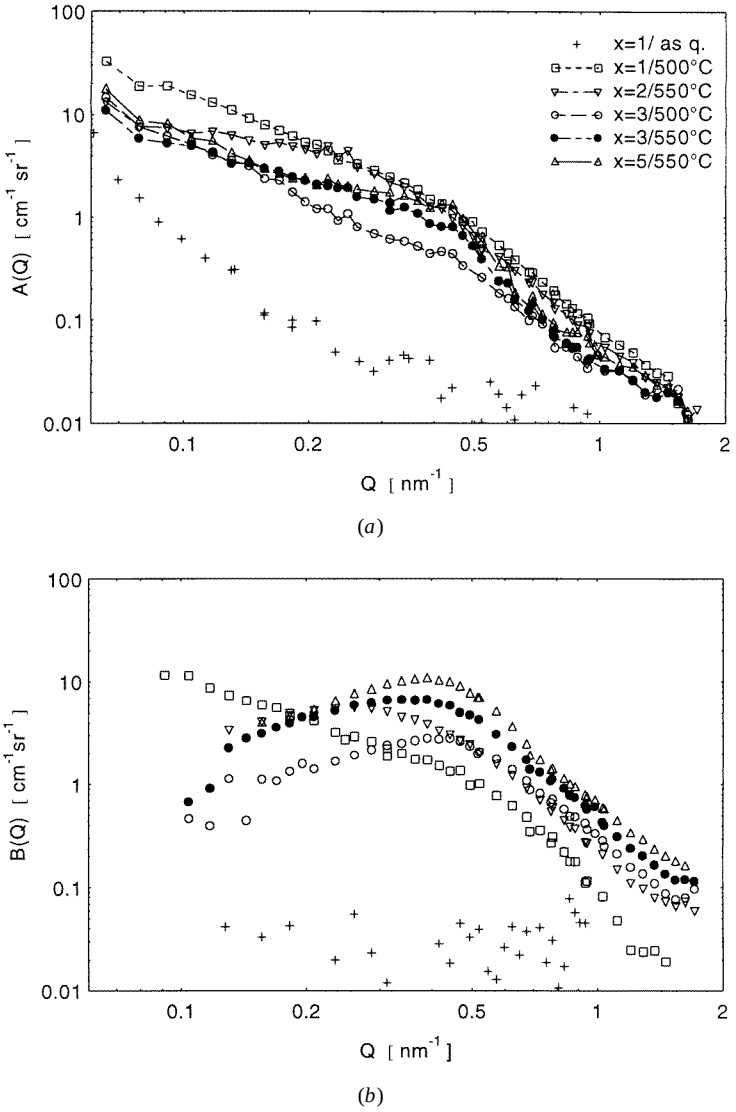

Figure 2. Isotropic and anisotropic scattering curves (*a*) $A(Q)$ and (*b*) $B(Q)$ in magnetic saturation ($B = 1$ T) for $Fe_{76.5-x}Si_{15.5}B_7CuNb_x$ after 1 hour annealing at different temperatures.

$Q > 0.5$ nm^{-1} only small changes were found. From the x-ray results it is known that the number density of precipitates increases with the annealing temperature. Thus the number of scattering waves to be superimposed increases and the interference becomes more dominant. The absence of the interference peak for $Fe_{75.5}Si_{15.5}B_7CuNb_1$ indicates that the short range order is significantly different from the other samples. We assume that clustering of particles occurs. From simulations [13] it is known that clustering of particles suppresses the interference. By means of transmission electron microscopy clustering was confirmed in partially crystallized $Fe_{76}Si_{15.5}B_7Nb_{1.5}$ [14]. We checked all scattering curves for $Q > 0.7$ nm^{-1} with respect to their asymptotic behaviour $I(Q) \approx Q^{-n}$. In contrast to [23] we found no evidence for $n = -2$ or -3. Best agreement was observed for $n = -4$ which corresponds to the Porod law for particles with smooth surfaces.

3.2.2. Simulation of interference and density profiles. We simulated the scattering signal of a system consisting of N spherical precipitates with Gaussian size distribution $N(R) \sim \exp[-\ln(2)(R - R_0)^2/\sigma^2]$. We generated 10 000 randomly distributed and nonoverlapping spheres inside a spherical matrix starting with the largest particles. A single spherical particle j at position $\boldsymbol{r}_j$ with radius R_j and scattering contrast $\Delta\eta_P$ relative to the matrix is characterized by the scattering amplitude $A_j(Q, R_j, \Delta\eta_P) = 4\pi\Delta\eta_P[\sin(QR_j) - QR_j\cos(QR_j)]/Q^3$. The total scattering intensity is then given by:

$$I(\boldsymbol{Q}) \propto \sum_j \sum_k A_j A_k^* \exp[-\mathrm{i}\boldsymbol{Q}\cdot(\boldsymbol{r}_j - \boldsymbol{r}_k)]. \tag{2a}$$

In figure 3 the results are presented for various volume fractions x_c of particles with typical parameters $R_0 = 7$ nm and $\sigma = 2$ nm. The solid line corresponds to a diluted system with the same size distribution and was calculated from:

$$I(Q) \propto \sum_j A_j A_j^*. \tag{2b}$$

In this context diluted means that all particles are widely separated and the scattered intensity of the complete system is the sum of scattering by N single particles. The diluted system is characterized by a monotonic increase in intensity for decreasing Q. In the range $Q > 0.4$ nm^{-1} the intensity increases rapidly. The oscillations known from monodisperse spheres are smeared out due to the broad size distribution. The curves obtained with (2*a*) deviate for $Q < 0.3$ nm^{-1} from this behaviour resulting from interference of neutrons scattered from neighbouring particles. The interference reduces the intensity for small Q and creates a maximum in the scattering curve. The higher the volume fraction of particles is, the more pronounced becomes this effect. The interference phenomenon is sensitive to the short range order. The range $Q > 0.5$ nm^{-1} is not affected by interference and allows the determination of the size distribution.

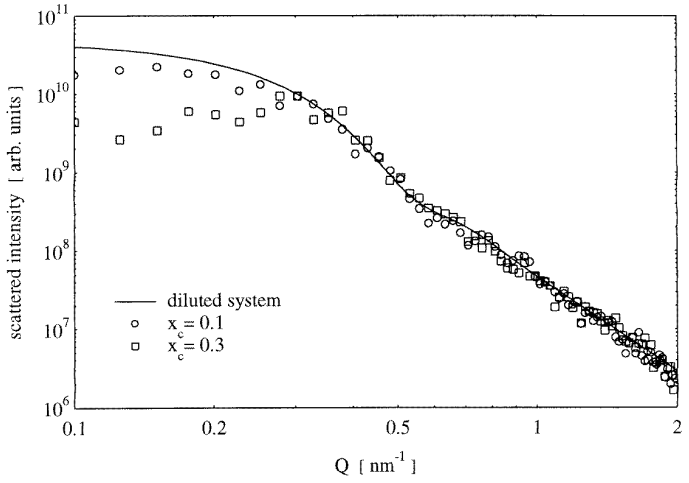

Figure 3. Simulated scattering curves for a system of spheres with Gaussian size distribution and various volume fractions of the particles.

In the next step we took into consideration a depletion zone around the precipitates. Niobium is insoluble in the crystalline phase. Therefore it is thought that Nb enriches around the particles. For a simple model of a homogeneous shell with thickness δ and

scattering contrast $\Delta\eta_S$ relative to the matrix the scattering amplitude of a single particle is modified by

$$\tilde{A}_j(Q, R_j, \Delta\eta_P, \delta, \Delta\eta_S) = A_j(Q, R_j, \Delta\eta_P - \Delta\eta_S) + A_j(Q, R_j + \delta, \Delta\eta_S). \tag{3}$$

This corresponds with the superposition of two spheres with identical centre $\boldsymbol{r}_j$ but different radii R_j $(R_j + \delta)$ and scattering contrast $\Delta\eta_M - \Delta\eta_S$ $(\Delta\eta_S)$. Figure 4 shows the scattering curves for a diluted system calculated from (2*b*) and (3) for $\delta = 1$ nm in dependence on the relative contrast $C = \Delta\eta_S/\Delta\eta_M$ for monodisperse and polydisperse spherical precipitates. The shell leads for negative C to a reduction of the scattered intensity for $Q < 0.5$ nm^{-1}. That means the shell amplifies the interference peak. If we consider that only iron atoms act as magnetic moments and assume similar density, then the crystallites have positive

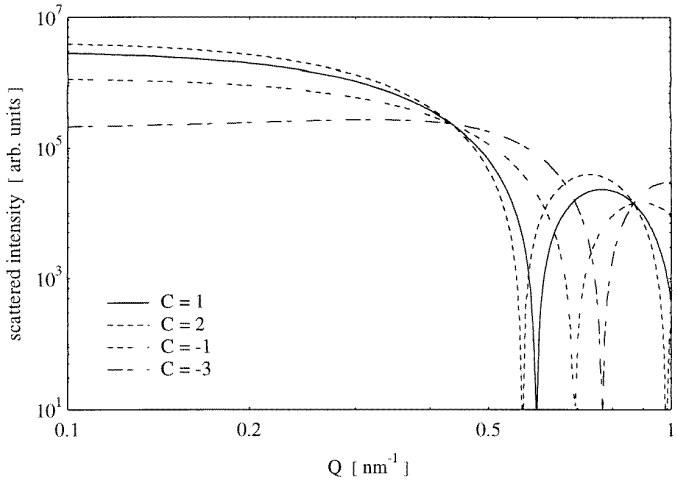

(*a*)

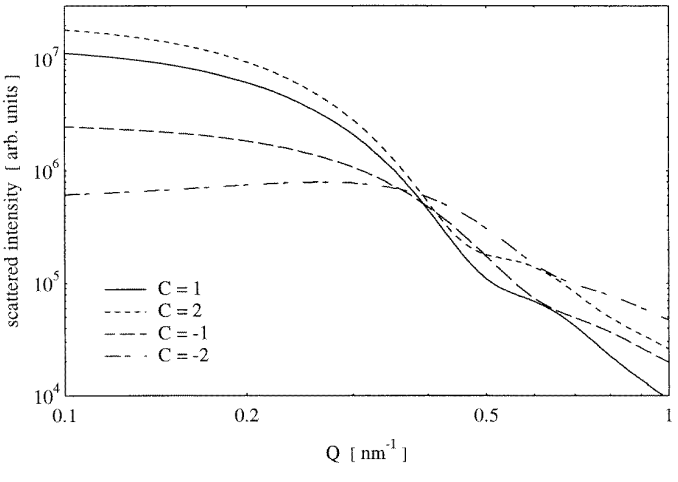

(*b*)

Figure 4. Simulated scattering curves for a diluted system of spheres with a thin shell in dependence on the relative contrast C for (*a*) monodisperse ($R = 7$ nm) and (*b*) Gaussian size distribution with typical parameters $R_0 = 7$ nm and $\sigma = 2$ nm.

magnetic contrast relative to the matrix, whereas the shell is characterized by negative magnetic contrast. This correlates with negative C and could explain the amplification of the interference peak in magnetic scattering. Since the nuclear scattering length densities of shell and matrix are very similar the effect of the density profile is less pronounced in $A(Q)$. This could explain the observed differences in $A(Q)$ and $B(Q)$. The correlation between niobium concentration and Curie temperatures observed in amorphous alloys [15, 16] is one more hint that the magnetization should be very sensitive to the shell. More realistic concentration profiles for the depletion region give the same effect [17]. Without the shell the asymptotic behaviour follows as expected the Porod law $I(Q) \approx Q^{-4}$; the depletion zone causes deviations.

3.2.3. Size distributions. From magnetic and nuclear scattering we determined particle size distributions by means of inverse Fourier transformation [18] under the assumption of homogeneous spherical particles. The spherical shape has been confirmed by TEM [5, 7, 14] in $Fe_{73.5}Si_{15.5}B_7CuNb_3$. No corresponding investigations are known for the remaining samples. X-ray measurements indicate that the microstructure for $x = 2$ and 5 at.% is very similar to that of $x = 3$ at.%. Samples without niobium show a more complex microstructure [14]. For $Fe_{75.5}Si_{15.5}B_7CuNb_1$ therefore the assumption of spherical particles is not guaranteed. In order to avoid the influence of interference only data points with $Q > 0.5$ nm^{-1} were used which restricts the observable particle size to the range between 3 and 15 nm. The Fourier transform leads to the volume distributions of spheres weighted with the squared scattering contrast as function of the radius R. Assuming that the scattering contrast is not a function of R the curves were renormalized to the total crystalline volume V_c determined from x-ray diffraction. For a given radius $V(R)N(R)/V_c$ describes the incremental volume fraction of particles with radius R.

From nuclear scattering asymmetric size distributions similar to log-normal type were derived (figure 5). The position of the maximum varies between 3 and 5 nm depending on sample composition and annealing conditions. Only in the sample with the lowest Nb amount of 1at.% were particles with a radius higher than 10 nm observed. The present results yield lower particle sizes than the XRD results and TEM investigations [5]. The behaviour derived from the magnetic scattering curves $B(Q)$ is very similar, but for the samples with $x \geqslant 3$ at.% the distributions are broadened and split into two peaks with maxima at $R =$ (3–5) nm and $R \approx 7$ nm. The first peak occurs at the same position as the maximum of the distribution derived from $A(Q)$. The second peak might be masked by the asymmetric shape in the curves obtained from $A(Q)$. If we exclude artefacts from the Fourier transform as the reason for the different shapes of the distributions derived from $A(Q)$ and $B(Q)$, then we have to answer the question of the physical background. From the different influence of the interference we have already found a hint that the existing fluctuations affect nuclear and magnetic scattering with different sensitivity. In particular, the samples with higher amount of niobium show asymmetric size distributions derived from $A(Q)$ and bimodal distributions derived from $B(Q)$. Even in these samples the assumed Nb enriched shell should influence scattering. As mentioned above, a spherical particle surrounded by a shell with different scattering contrast has the same form factor as the superposition of two spheres with different scattering contrast and radii. The size distribution for such composite particles is only reproduced from scattering curves by using the correct scattering amplitude. However, the present evaluation of $R^3N(R)$ required homogeneous particles. The corresponding size distributions then must contain additional contributions from larger particles representing sphere and shell. This might be an explanation for the

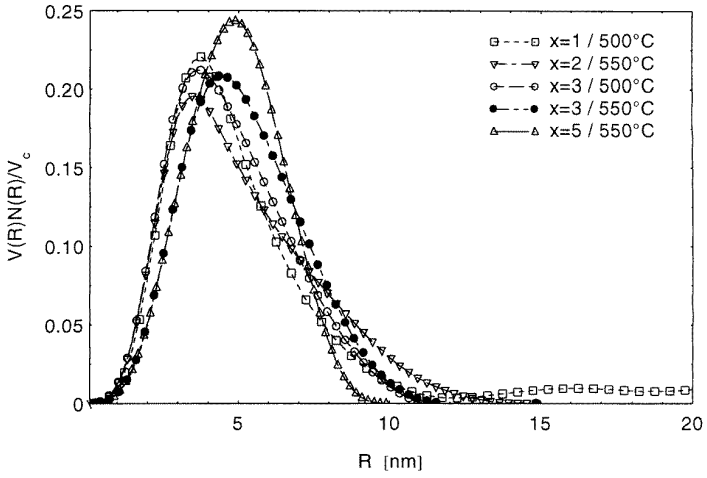

(*a*)

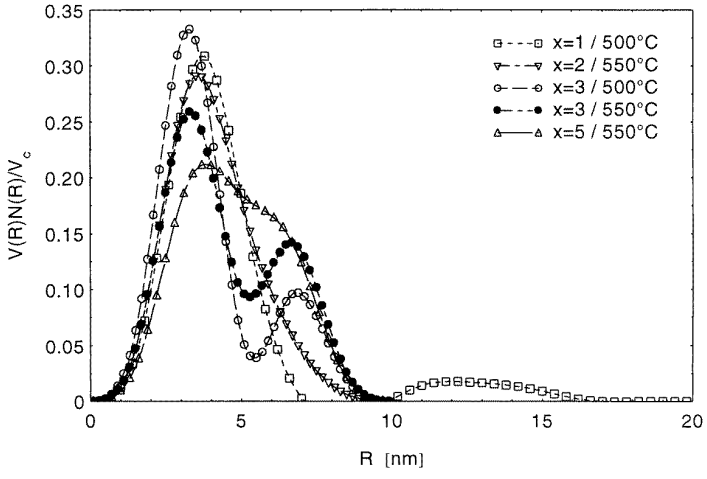

(*b*)

Figure 5. Renormalized size distributions of precipitates in $Fe_{76.5-x}Si_{15.5}B_7CuNb_x$ determined from (*a*) $A(Q)$ and (*b*) $B(Q)$.

split size distributions. If nuclear scattering density is actually less sensitive to this shell, then the effect is less pronounced in the nuclear scattering.

3.2.4. Magnetic contrast. For a two phase system the scattering invariant K is related to the volume fractions x_1 and x_2 of the phases and the scattering contrast $\Delta\eta$ between them by [19]:

$$K \equiv V^{-1}\int_0^\infty I(Q)Q^2\,\mathrm{d}Q = 2\pi^2 x_1 x_2 |\Delta\eta|^2. \tag{4}$$

For systems with magnetic scattering contribution two appropriate invariants K_n and K_m with respect to nuclear and magnetic scattering can be defined in magnetic saturation. $I(Q)$ in (4) has to be replaced by $A(Q)$ and $B(Q)$. For nuclear scattering $\Delta\eta$ corresponds to

the difference in the nuclear scattering length density of the phases, whereas for magnetic scattering it is proportional to the difference in the magnetization ΔM.

We evaluated K_n and K_m for all samples which allows us to determine magnetic and nuclear contrasts provided the volume fractions are known. However, due to uncertainties in the absolute values of the intensities we rather compare the ratio K_m/K_n (table 2) for samples of different composition and volume fraction. On the other hand from previous investigations the composition of the crystalline phase is known as a function of annealing temperature and composition of the as-quenched alloy [5, 20]. Using the lever rule and the crystalline volume fractions from x-ray measurements the average composition of the remaining amorphous phase can be estimated (column 4 in table 2). A correlation between the amount of Nb and the ratio K_m/K_n is found. In the alloys $Fe_{75.5}Si_{15.5}B_7CuNb_1$ and $Fe_{74.5}Si_{15.5}B_7CuNb_2$ with the same crystalline volume fraction K_m/K_n increases with the amount of Nb from 1.2 to 3.1. The remaining amorphous phase differs mainly in the amount of Nb, which reduces the density of magnetic iron atoms. Therefore the magnetic contrast between crystalline and amorphous phase increases with higher amount of Nb. For the alloys with $x = 3$ and 5 at.% Nb the ratio K_m/K_n reaches even higher values between 8.9 and 11.1 for different values of the crystalline volume fraction although the amount of Nb in the remaining matrix (table 2) seems to be similar to that in the samples with $x = 1$ and 2 at.%. This observed tendency in K_m/K_n cannot be produced from variations in the nuclear contrast alone. Instead, we assume that the Nb enriched shell around the crystals amplifies the magnetic contrast between crystals and matrix and modifies the magnetic coupling leading to a strong decrease of the Curie temperature [15].

Table 2. Ratio K_m/K_n of magnetic and nuclear scattering invariant for various alloys with crystallization degree x_c.

Alloy	x_c	K_m/K_n	Composition of remaining amorphous phase
$Fe_{75.5}Si_{15.5}B_7CuNb_1$	0.78	1.2	$Fe_{59}B_{32}Cu_{4.5}Nb_{4.5}$
$Fe_{74.5}Si_{15.5}B_7CuNb_2$	0.78	3.1	$Fe_{55}B_{32}Cu_{4.3}Nb_{8.6}$
$Fe_{73.5}Si_{15.5}B_7CuNb_3$	0.38	9.5	$Fe_{70.5}Si_{11.8}B_{11.3}Cu_{1.6}Nb_{4.8}$
$Fe_{73.5}Si_{15.5}B_7CuNb_3$	0.45	8.9	$Fe_{69.6}Si_{10.6}B_{12.7}Cu_{1.8}Nb_{5.4}$
$Fe_{73.5}Si_{15.5}B_7CuNb_3$	0.67	10.8	$Fe_{63.3}Si_{3.3}B_{21.2}Cu_3Nb_9$
$Fe_{71.5}Si_{15.5}B_7CuNb_5$	0.45	11.1	$Fe_{65.7}Si_{10.6}B_{12.7}Cu_{1.8}Nb_9$

4. Summary

We performed SANS on partially crystallized $Fe_{76.5-x}Si_{15.5}B_7CuNb_x$ alloys. From nuclear and magnetic scattering we calculated the particle size distributions for spherical precipitates. The maximum of the volume weighted size distributions varied between 3 and 5 nm dependent on composition and annealing conditions of the alloy. Only for the alloy $Fe_{75.5}Si_{15.5}B_7CuNb_1$ was a significant number of particles with radius $R > 10$ nm observed. Whereas size distributions determined from nuclear scattering are similar to log-normal shape, the magnetic scattering for samples with $x \geqslant 3$ at.% indicates a bimodal size distribution. From both nuclear and magnetic scattering curves we determined the invariants K_m and K_n. The ratio K_m/K_n is correlated with the amount of Nb in the alloy. This behaviour, the differences in the particle size distributions derived from nuclear and magnetic scattering and the maxima observed in the magnetic scattering contributions can be explained

by a microstructure of spherical crystallites surrounded by a Nb enriched shell. In fact, first systematic investigations of the magnetic scattering behaviour around the Curie temperature of the matrix gave evidence [21] of the existence of the shell and the influence on the magnetic coupling between the nanoparticles. To prove our assumptions further scattering experiments at different temperatures are in progress. Because of the different Curie temperatures T_C^p, T_C^s and T_C^m of particles, shell and matrix with $T_C^p > T_C^m > T_C^s$ it is possible to vary the influence of the shell on magnetic scattering. For $T < T_C^s$ the neutrons 'see' with respect to the magnetic interaction three phases, but for $T_C^p > T > T_C^m$ both matrix and shell become nonmagnetic. In $Fe_{73.4}Si_{13.4}B_{9.1}CuNb_3$ [22] evidence for a parabolic law for diffusion controlled crystal growth was found in the early stage of crystallization. The diffusion barrier stops the growth. Nucleation occurs homogeneously. In [5] the crystallization in $Fe_{73.5}Si_{15.5}B_7CuR_3$ was simulated with a parabolic growth law modified with respect to the diffusion barrier and exponential increase of the number of nuclei. The time dependence of the crystalline volume fraction and the mean particle size derived from time resolved x-ray diffraction was reproduced with this model. The broad size distributions from the SANS investigations indicate that local fluctuations in the as-quenched state initiate spatial variations of the asymptotic reached particle size. Further SANS investigations would help to prove this picture in detail from the time dependence of the size distributions.

References

[1] Yoshizawa Y, Oguma S and Yamauchi K 1988 *J. Appl. Phys.* **64** 6044
[2] Müller M, Mattern N and Illgen L 1992 *J. Magn. Magn. Mater.* **112** 263
[3] Herzer G 1991 *Mater. Sci. Eng.* A **133** 1
[4] Yoshizawa Y and Yamauchi K 1990 *Mater. Trans. JIM* **31** 307
[5] Danzig A 1996 *Thesis* TU Dresden (Aachen: Shaker)
[6] Yoshizawa Y and Yamauchi K 1991 *Mater. Sci. Eng.* A **133** 176
[7] Hiraga K and Kohmoto O 1991 *Mater. Trans. JIM* **33** 868
[8] Kulik T 1992 *Mater. Sci. Eng.* A **159** 95
[9] Müller M and Mattern N 1994 *J. Magn. Magn. Mater.* **136** 79
[10] Keiderling U and Wiedenmann A 1995 *Physica* B **213/214** 895
[11] Matyi R J, Schwartz L H and Butt J B 1987 *Catal. Rev. Sci. Eng.* **29** 41
[12] Kostorz G 1991 *J. Appl. Crystallogr.* **24** 444
[13] Uebele P and Hermann H 1996 *Modelling Simul. Mater. Sci. Eng.* **4** 203
[14] Klement U, Mattern N and Müller M 1995 *Proc. 1995 Int. Symp. on Metastable, Mechanically Alloyed and Nanocrystalline Materials (Quebec, 1995)*, 1996 *Mater. Sci. Forum* **225–227** 683
[15] Yavari A R and Drbohlav O 1995 *Mater. Trans. JIM* **36** 896
[16] Müller M, Mattern N and Illgen L 1991 *Z. Metall. kd.* **82** 895
[17] Kranold G and Walter R 1990 *Physical Research* vol 12 ed D Schulze (Berlin: Akademie) pp 267ff
[18] Glatter O 1981 *J. Appl. Crystallogr.* **14** 101
[19] Williams C E, May R P and Guinier A 1991 *Materials Science and Technology* vol 12, ed R W Cahn, P Haasen and E J Kramer (Weinheim: VCH) ch 20
[20] Danzig A and Mattern N 1995 *Phys. Status Solidi* a **147** 335
[21] Kohlbrecher J, Wiedenmann A and Wollenberger 1997 *Z. Phys.* **1** 100
[22] Köster U and Schünemann U 1991 *Mater. Sci. Eng.* A **133** 611
[23] Ohnuma M, Suzuki J, Funahashi S, Ishigaki T, Kuwano H and Hamaguchi Y 1995 *Physica* B **213/214** 582